Instability growth rate of two-phase mixing layers from a linear eigenvalue problem and an initial-value problem

Anne Bagué,[1] Daniel Fuster,[1] Stéphane Popinet,[2] Ruben Scardovelli,[3] and Stéphane Zaleski[1,a)]
[1]*University Paris 06 and CNRS, UMR 7190, Institut Jean Le Rond d'Alembert, Paris F-75005, France*
[2]*National Institute of Water and Atmospheric Research, P.O. Box 14-901, Kilbirnie, Wellington, New Zealand*
[3]*DIENCA-Lab. di Montecuccolino, University of Bologna, Bologna, Italy*

(Received 7 May 2010; accepted 21 June 2010; published online xx xx xxxx)

The temporal instability of parallel two-phase mixing layers is studied with a linear stability code by considering a composite error function base flow. The eigenfunctions of the linear problem are used to initialize the velocity and volume fraction fields for direct numerical simulations of the incompressible Navier–Stokes equations with the open-source GERRIS flow solver. We compare the growth rate of the most unstable mode from the linear stability problem and from the simulation results at moderate and large density and viscosity ratios in order to validate the code for a wide range of physical parameters. The efficiency of the adaptive mesh refinement scheme is also discussed. © *2010 American Institute of Physics*. [doi:10.1063/1.3483206]

I. INTRODUCTION

Two-phase mixing layers are easily found in nature and industrial applications. Typical phenomena are the formation of sea waves by the wind and fuel atomization. In particular, the breakup of a liquid jet in thermal engines is a very complex phenomenon investigated by many research groups as the atomization process is important for the combustion quality, engine efficiency, and pollutant emission. A number of mechanisms have been proposed that may lead ultimately to ligament and droplet formation. A high level of turbulent eddies upstream of the nozzle may have sufficient energy to overcome the stabilizing effect of surface tension and to create ligaments directly, while a lower level may give rise to interface perturbations that are unstable, in this case the gas phase plays an essential role. In the second situation, planar models are likely to be relevant to jet instabilities at the early stages of the interface evolution near the nozzle exit where the observed spatial scale of the instability is small compared to the jet radius.

This paper focuses on the direct numerical simulation of unstable perturbations in two-phase mixing layers in a two-dimensional Cartesian geometry and in circumstances in which the turbulent eddies upstream of the nozzle are of sufficiently small amplitude so that linearized analysis may apply. This is in particular the case of a number of experiments specially designed to reduce the turbulence level.[1] This phenomenon was first investigated by Kelvin and Helmholtz in the 19th century who developed the single-phase inviscid theory. At the beginning of the 20th century, Heisenberg, Lin, Tollmien, and Schlichting found how the viscosity modifies and contributes to the inviscid perturbations.[2] Later on Yih found that for two different fluid phases a viscosity contrast can give rise to an interfacial mode for long waves.[3] Finally, Hooper and Boyd[4] observed other effects at small Reynolds numbers which have been explained by Hinch.[5]

Up to now, a limited number of direct numerical simulations of the Navier–Stokes equations for two-phase mixing layers have been performed. Some preliminary results using the Volume of Fluid (VOF) method have been presented by Keller,[6] Li,[7] and Leboissetier.[8] Other two-dimensional simulations of the Navier–Stokes equations have been performed by Tauber[9] using an interface front tracking method.

Linear stability analysis of viscous modes in two-phase mixing layers has been performed by a number of authors. In this paper we use the results obtained by Yecko[10] and Boeck[11] who considered in their linear problem a base flow composed by error function profiles in each fluid layer. The eigenfuctions from their analysis are used to initialize the interface and velocity profile, while the growth rate of the most unstable mode is compared with the value from the direct numerical simulations.

To perform the simulations presented in this work we use the numerical code GERRIS,[12] an open-source flow solver (http://gfs.sf.net). The incompressible single-fluid formulation of the Navier–Stokes equations is simplified with a classical time-splitting projection method and the resulting Poisson equation for the pressure is solved with a multigrid technique. The model implements adaptive mesh refinement (AMR), which is based on a quad/octree spatial discretization with automatic and dynamic local refinement according to different physical criteria. A VOF/PLIC algorithm has been implemented to reconstruct the interface and a direction-split technique to advect the volume fraction function. Continuous surface force (CSF) is combined with the height function method[13] to model surface tension.[14] Some preliminary results about the validation of this code through comparison with the viscous linear theory have been presented previously.[15]

The structure of the paper is as follows. In the following section we discuss the linear eigenvalue problem including

a)Electronic mail: stephane.zaleski@upmc.fr.

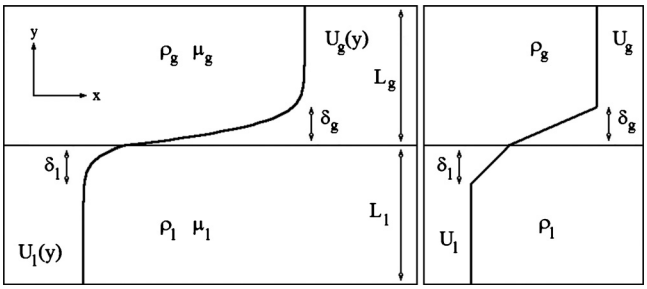

FIG. 1. Parameters and base flow profiles used in the liquid and gas phases for the viscous (left) and inviscid (right) linear stability problems.

the velocity distribution of the base flow and the inviscid and viscous linear stability equations. Next we describe the initial conditions of the direct numerical simulations obtained from the eigenfunctions of the linear stability problem and how we compute the growth rate of the instability from the simulation data. Then we present the results at moderate and large density and viscosity ratios discussing how the instability wavenumber and the surface tension coefficient affect the convergence of the simulations. Finally we discuss the efficiency of AMR and present our conclusions.

II. BASE FLOW AND LINEAR STABILITY PROBLEM

In experiments on atomization wavy perturbations of the liquid-gas interface grow away from the nozzle, evolving into liquid sheets that by three-dimensional destabilization may develop ligaments that eventually break up into droplets.[16] The velocity field near the interface is characterized by a boundary layer of different size in each phase, which develops further on with the downstream distance from the nozzle exit. In order to neglect the spatial evolution of the base flow and to approximate the physical problem as the temporal evolution of a spatially periodic flow, one has to resort to the parallel flow assumption. The consistency of this assumption requires the cross-stream velocity component to be negligible compared to the streamwise component and the predicted unstable wavelength to be much smaller than the downstream distance over which the boundary layer thickness changes significantly. Both requirements can be satisfied within the usual assumptions of boundary layer theory, namely, when the Reynolds number based on the downstream distance is large.[17] We also remark that the stability results for sinusoidal streamwise perturbations are related to spatially growing perturbations by Gaster's transformation provided the growth over one oscillation period is sufficiently small.[18]

In this paper we are interested in the amplification of wavy two-dimensional perturbations of a liquid-gas interface which is initially flat, hence not too far away from the nozzle. The base flow will be approximated by a parallel flow, as schematically illustrated on the left of Fig. 1. The stability of this flow will be studied as a linear eigenvalue problem and the eigenfunctions corresponding to a given wave number will be used to initialize a perturbation of the base flow. The perturbed initial state will be followed in time by the numerical code GERRIS in order to compare the two growth rates.

The self-similar velocity profile of the base flow has been computed by Lock[19] using the boundary layer theory for a two-phase flow. Even if there is no analytical solution of the nonlinear boundary layer equations, an analytical tanh-profile has been considered as a good approximation of the base flow for stability calculations in the one-phase problem.[20] Therefore, as in previous works,[10,11] we consider an error function profile for both phases. The argument of the error function is scaled by the boundary layer thickness in each phase and the zero is located on the stationary interface line (see Fig. 1). The shape of the numerical solutions of Ref. 19 are well approximated by such error functions, while stability results based on the exact profiles of Lock's problem have been compared with those based on the error function profile in Ref. 21.

A. Velocity distribution of the base flow

In the comoving reference frame where the velocity is zero on the stationary interface, the analytical expressions for the parallel base flow are

$$U_l(y) = U_l^* \operatorname{erf}(y/\delta_l) \quad (y<0), \tag{1}$$

$$U_g(y) = U_g^* \operatorname{erf}(y/\delta_g) \quad (y>0), \tag{2}$$

where the subscripts l and g denote liquid and gas (or more generally two fluids with different physical properties) and the interface coincides with the coordinate axis $y=0$.

The two asymptotic velocities, U_l^* and U_g^*, and the boundary layer thicknesses, δ_l and δ_g, are not independent parameters since they are coupled by the shear stress continuity at the interface. Thus, by using Eqs. (1) and (2) the following relation is established:

$$\frac{\mu_l U_l^*}{\delta_l} = \frac{\mu_g U_g^*}{\delta_g}. \tag{3}$$

Nondimensional physical and geometrical parameters of the problem are the density, viscosity, and thickness ratios,

$$r = \frac{\rho_g}{\rho_l}, \quad m = \frac{\mu_g}{\mu_l}, \quad n = \frac{\delta_g}{\delta_l}. \tag{4}$$

To define other dimensionless numbers we need a reference velocity and length. A convenient choice is the asymptotic velocity U_g^* and boundary layer thickness δ_g of the gas phase. With these two reference scales we define the Reynolds and Weber numbers for the liquid and gas phases as

$$\mathrm{Re}_l = \frac{\rho_l U_g^* \delta_g}{\mu_l}, \quad \mathrm{Re}_g = \frac{\rho_g U_g^* \delta_g}{\mu_g},$$

$$\mathrm{We}_l = \frac{\rho_l (U_g^*)^2 \delta_g}{\sigma}, \quad \mathrm{We}_g = \frac{\rho_g (U_g^*)^2 \delta_g}{\sigma}, \tag{5}$$

where σ is the constant surface tension coefficient.

B. Inviscid and viscous eigenvalue problem

The linear stability problem is formulated in two dimensions and without gravity for both phases. The perturbations of the base flow are written in terms of the streamfunctions ψ_l and ψ_g, as in Refs. 10 and 11. The streamwise and cross-stream velocity components u and v are defined by

$$u = \partial_y \psi, \quad v = -\partial_x \psi \tag{6}$$

in both phases. Since the unperturbed flow does not depend on time t and streamwise coordinate x, the linearization of the dynamical problem about the base velocity profile implies that the solution can be written as

$$\psi_l(x,y,t) = \phi_l(y)\exp[i\alpha(x-ct)] \quad (y<0), \tag{7}$$

$$\psi_g(x,y,t) = \phi_g(y)\exp[i\alpha(x-ct)] \quad (y>0). \tag{8}$$

With this *ansatz* and proper boundary conditions, we obtain an eigenvalue problem for the two ordinary differential equations in ϕ_l and ϕ_g. The real wavenumber α should be considered as a parameter, while the complex eigenvalues $c=c_r+ic_i$ determine the phase velocity c_r and growth rate (αc_i) of the modes.

In the inviscid case, from the linearized momentum equation, one derives the following differential equations for the liquid and gas phases:

$$(U_l-c)(D^2-\alpha^2)\phi_l - D^2U_l\phi_l = 0, \tag{9}$$

$$(U_g-c)(D^2-\alpha^2)\phi_g - D^2U_g\phi_g = 0, \tag{10}$$

where D is the differential operator along the cross-stream coordinate y. The boundary conditions at the interface $(y=0)$ are the continuity of the normal component of the velocity v and the pressure

$$\phi_l = \phi_g, \tag{11}$$

$$-\frac{\alpha^2}{rc\ \mathrm{We}_l}\phi_l = \frac{1}{r}(cD\phi_l + DU_l\phi_l) - (cD\phi_g + DU_g\phi_g). \tag{12}$$

Analytical solutions of Eqs. (9)–(12) can be found when the second derivative of the base flow U is zero, i.e., for base velocity profiles composed by a chain of consecutive segments, as shown on the right of Fig. 1. In this case the solution is a linear combination of the exponential functions $\exp(\pm\alpha y)$. The same boundary conditions (11) and (12) should be applied at the intersection of two consecutive segments. The whole problem is reduced to an algebraic eigenvalue problem for c. The roots of the characteristic polynomial can be computed with standard software packages.

In the viscous case, the linearized momentum equation gives rise to the well-known fourth-order Orr–Sommerfeld equation for each phase

$$(U_l-c)(D^2-\alpha^2)\phi_l - D^2U_l\phi_l = \frac{1}{i\alpha\ \mathrm{Re}_l}(D^2-\alpha^2)^2\phi_l, \tag{13}$$

$$(U_g-c)(D^2-\alpha^2)\phi_g - D^2U_g\phi_g = \frac{m}{r}\frac{1}{i\alpha\ \mathrm{Re}_l}(D^2-\alpha^2)^2\phi_g. \tag{14}$$

The higher order of the differential equations leads to additional conditions at the interface, where we require the continuity of the normal and tangential components of the velocity

$$\phi_l = \phi_g, \tag{15}$$

$$\left(D+\frac{1}{c}DU_l\right)\phi_l = \left(D+\frac{1}{c}DU_g\right)\phi_g, \tag{16}$$

and that of the normal and tangential stresses as well

$$-\frac{\alpha^2}{rc\ \mathrm{We}_l}\phi_l = \frac{1}{r}(cD\phi_l + DU_l\phi_l) + \frac{1}{i\alpha r\ \mathrm{Re}_l}\times(D^3\phi_l - 3\alpha^2 D\phi_l) - (cD\phi_g + DU_g\phi_g) - \frac{m}{i\alpha r\ \mathrm{Re}_l}(D^3\phi_g - 3\alpha^2 D\phi_g), \tag{17}$$

$$\left(D^2+\alpha^2+\frac{1}{c}D^2U_l\right)\phi_l = m\left(D^2+\alpha^2+\frac{1}{c}D^2U_g\right)\phi_g. \tag{18}$$

The viscous eigenvalue problem for the error function profile can only be solved numerically. For the geometry shown in Fig. 1 it is possible to introduce two semi-infinite mappings to push the top and bottom boundary conditions to infinity, see for example Ref. 22. Alternatively, one can set a boundary condition at some large but finite cross-stream distance from the interface. Therefore, we place two rigid walls at $y=-L_l$ and $y=L_g$, where the fluid velocity is equal to zero

$$\phi_l = D\phi_l = 0 \quad (y=-L_l), \tag{19}$$

$$\phi_g = D\phi_g = 0 \quad (y=L_g). \tag{20}$$

In the inviscid case only the normal component of the velocity is zero. We remark that L_l and L_g should be sufficiently large in order to ensure the independence of the results from their values.[10,11] With this geometry, the initialization of the nonlinear Navier–Stokes solver GERRIS is straightforward.

The linear stability problem for the complex eigenvalue c, with given physical and geometrical parameters and wavenumber α in the domain $-L_l \le y \le L_g$, is solved numerically by using a Chebyshev collocation method.[10,23,24] Each fluid subdomain, $[-L_l,0]$ and $[0,L_g]$, is transformed into the interval $[-1,1]$, by a different linear transformation of the independent variable y. The eigenfunctions ϕ_l and ϕ_g are expanded in Chebyshev polynomials and are evaluated at prescribed collocation points, here the extrema of the highest order polynomial, in order to ensure spectral accuracy.[23,25] In the resulting linear algebraic system for the coefficients of the Chebyshev polynomials, the eigenvalue c is considered as a parameter, and the system is resolved with the QZ-algorithm[26] implemented in the NAG library. At the end of the calculation, the eigenfunctions are normalized in such a way that the maximum coefficient is equal to 1. For a given set of physical and geometrical parameters and wavenumber

AQ: #4

TABLE I. Physical and geometrical parameters of the base flow profiles.

Case	m	r	δ_l/L_l	δ_g/L_g	Re_l	Re_g	We_l	We_g
A	0.1	1	1/6	1/6	200	2000	∞	∞
B	0.1	1	1/6	1/6	200	2000	10	10
C	0.99	0.1	1/6	1/6	19 800	2000	∞	∞
D	0.99	0.1	1/6	1/6	19 800	2000	100	10

α, several unstable modes with different growth rates may be found. A detailed analysis of these modes and of the physical mechanisms driving the instability can be found in Ref. 11. In this paper we focus only on the most unstable mode.

III. SIMULATIONS AT MODERATE DENSITY AND VISCOSITY RATIOS

In this section we present the results of the eigenvalue problem and the numerical simulations for cases where the density and viscosity ratios are of the order of 10.

A. Base flow parameters

The four parameters U_l^*, U_g^*, δ_l, and δ_g are related by Eq. (3). Furthermore, we assume $\delta_l=\delta_g=L/6$, with $L=L_l=L_g$. Then, we need to specify only the reference velocity, $U_g^*=10$ m/s, and length, $\delta_g=2.5\times10^{-3}$ m. For all cases, the gas properties have the same value, with density $\rho_g=1$ kg/m^3 and viscosity $\mu_g=1.25\times10^{-5}$ kg/m s. The surface tension coefficient σ is either zero or 2.5×10^{-2} J/m^2.

In the first two cases *A* and *B* of Table I, the two fluids have the same density, $r=\rho_g/\rho_l=1$, but different viscosity, $m=\mu_g/\mu_l=0.1$. The other two cases, *C* and *D*, have almost the same viscosity, $m=0.99$, but a different density, $r=0.1$. With these values the adimensional numbers given in Table I are readily computed.

B. Eigenfunctions from linear stability theory

An important parameter to get accurate results in the linear eigenvalue problem is the number N of Chebyshev polynomials used in the expansion of the eigenfunctions ϕ_l and ϕ_g. We consider the same number of polynomials in the liquid and gas phases, i.e., $N=N_l=N_g$. The growth rate for the four cases of Table I is presented in Table II as a function of the integer N. For each case we observe a range of N where the growth rate remains roughly constant. To compute the eigenfunctions we consider the minimum value in this interval of N. Thus, for the four cases of Table I we have chosen $N=(70,70,100,100)$. Beyond this range of constant growth rate, round-off errors become important as the number N of polynomials is increased. Quadruple precision could be a way to overcome this issue.

Next, we examine the profile of the eigenfunctions. Figure 2 shows the real $\phi_r(y)$ and imaginary $\phi_i(y)$ parts of these functions for the cases *A* and *C* of Table I. The real part $\phi_r(y)$ of the eigenfunction is rather similar in the two cases, while the behavior of the imaginary part $\phi_i(y)$ is substantially different. For case *A*, with density ratio $r=1$ and viscosity ratio $m=0.1$, we observe a very sharp negative peak in the liquid phase ($y<0$) just across the interface, and a weaker and more round maximum in the gas phase ($y>0$). The opposite is found for case *C*, with density ratio $r=0.1$ and viscosity ratio $m=0.99$. There is a very large and round minimum in the liquid and a sharp but rather small maximum in the gas. Notice that the imaginary part of the eigenfunction changes its sign twice in the gas. The introduction of surface tension, at least in these two cases, does not change the shape of the eigenfunctions, but simply reduces the amplitude of its extremum.

TABLE II. Variation of the growth rate with the number N of Chebyshev polynomials for the four cases of Table I with $\alpha\delta_g=\pi/2$.

	Case			
N	*A*	*B*	*C*	*D*
40	**0.108**55398	**0.093**916996	1.5400230	**0.1**4058223
70	**0.10870**192	**0.09377**3774	**0.20**126900	**0.189**23558
90	**0.10870**175	**0.09377**3438	**0.20070**193	**0.18854**588
100	**0.10870**181	**0.09377**3482	**0.20069**428	**0.18853**798
120	**0.10870**161	**0.09377**3446	**0.20069**689	**0.18853**832
140	**0.10870**154	**0.09377**3649	**0.20069**848	**0.1885**0341
160	**0.10870**432	**0.09377**4442	**0.20069**865	**0.188**60924
190	**0.1087**1292	**0.09377**0611	**0.2007**1194	**0.19**463859

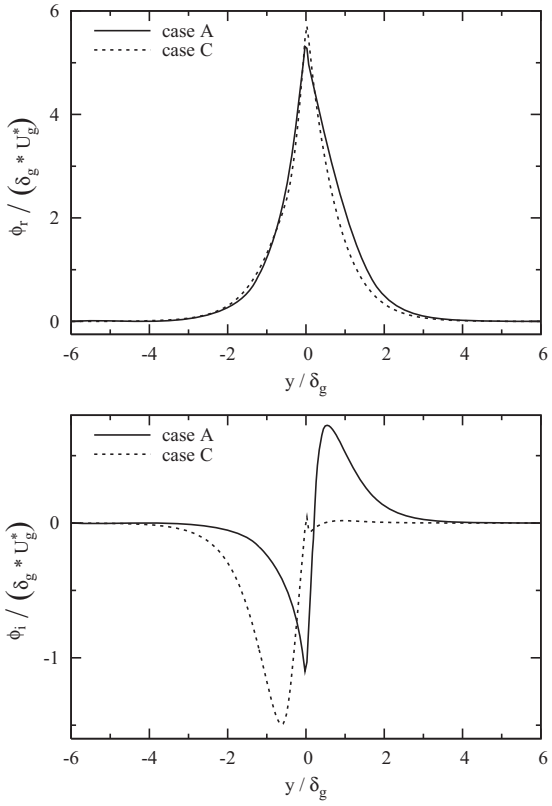

FIG. 2. Real (top) and imaginary (bottom) parts of the eigenfunction $\phi(y)=\phi_r(y)+i\phi_i(y)$ for cases *A* and *C* of Table I.

C. Growth rates from the linear stability theory and initial-value problem

Let us consider a rectangular domain defined by $-L<y<0$ for the liquid phase and $0<y<L$ for the gas phase, while in the streamwise coordinate x we take the horizontal length $L_x=2/3L$. The basic geometrical structures in the GERRIS code are squares, so our computational domain consists of three boxes in the vertical direction each of them with a maximum of 256^2 square cells. When we use AMR the maximum resolution has the same grid spacing, i.e., $h=L_x/256$. We consider an initial perturbation with a wavelength equal to L_x, then the wavenumber is $\alpha=2\pi/L_x$, and we change the adimensional wavenumber $\alpha\delta_g$ by varying the gas boundary layer thickness δ_g.

The velocity profile at the beginning of the simulation is the sum of the base profile, Eqs. (1) and (2), and a small perturbation derived from the complex streamfunctions ψ_g and ψ_l given by Eqs. (7) and (8),

$$u(x,y,t=0)=U(y)+\varepsilon[D\phi_r\cos(\alpha x)-D\phi_i\sin(\alpha x)], \tag{21}$$

$$v(x,y,t=0)=\varepsilon\alpha[\phi_i\cos(\alpha x)+\phi_r\sin(\alpha x)], \tag{22}$$

where $\varepsilon/U_g^*=10^{-3}$ is the amplitude of the perturbation. In the regime of linear growth rate, the results do not depend on this ratio. Its value is a simple numerical compromise between an appreciable size of the initial perturbation with respect to the grid spacing and a large temporal window of linear growth rate (as shown on the bottom of Fig. 3).

The displacement η of the interface from the base state is given by the equation

$$\partial_t\eta(x,t)=v(x,y=0,t)\rightarrow\eta(x,t)=i\frac{\alpha c^*v(x,0,t)}{|\alpha c|^2}, \tag{23}$$

where the v component of the velocity is evaluated at the initial time $t=0$. The real part of Eq. (23) allows us to obtain the initial interface displacement

$$\eta(x,t=0)=\frac{\varepsilon\alpha^2}{|\alpha c|^2}\{c_i[\phi_i\cos(\alpha x)+\phi_r\sin(\alpha x)] + c_r[\phi_r\cos(\alpha x)-\phi_i\sin(\alpha x)]\}, \tag{24}$$

which is used to initialize the volume fraction field C. Finally, we consider the harmonic mean of the viscosity,

$$\frac{1}{\mu}=\frac{C}{\mu_l}+\frac{1-C}{\mu_g}, \tag{25}$$

because this mean has been shown to give better results when the interface is parallel to the flow.[16]

We should remark that the initial sinusoidal displacement of the interface line is calculated from the solution, expressed as a series of Chebyshev polynomials, of the eigenvalue problem derived from the linearized Navier–Stokes equations, while the initial-value code GERRIS resolves the nonlinear Navier–Stokes equations with a finite volume approach. Furthermore the VOF/PLIC algorithm approximates the interface as a segment in each mixed cell and the capillary force calculation as well is affected by numerical errors that cause the well-known problem of spurious currents. All these issues may be the source of high-frequency disturbances that interact nonlinearly with each other and with the initial perturbation, which is the only unstable mode in the spectrum. However, these disturbances initially are indeed very small and they need time to develop appreciably. Therefore, in our simulations, we observe indeed an initial regime of linear growth rate and, in order to obtain the temporal evolution of the amplitude of the perturbation, we fit the interface line with the sinusoidal function $y=a\sin(2\pi x/L_x+b)+c$, as shown on the top of Fig. 3, where a, b, and c are three free parameters. We then estimate the growth rate of the instability as the slope of the amplitude a of the wave as a function of time t on a linear-log plot, in the region where a linear behavior is observed, as on the right of Fig. 3. This procedure is applied to the simulation data coming from GERRIS and the fixed-grid code SURFER.[27,28]

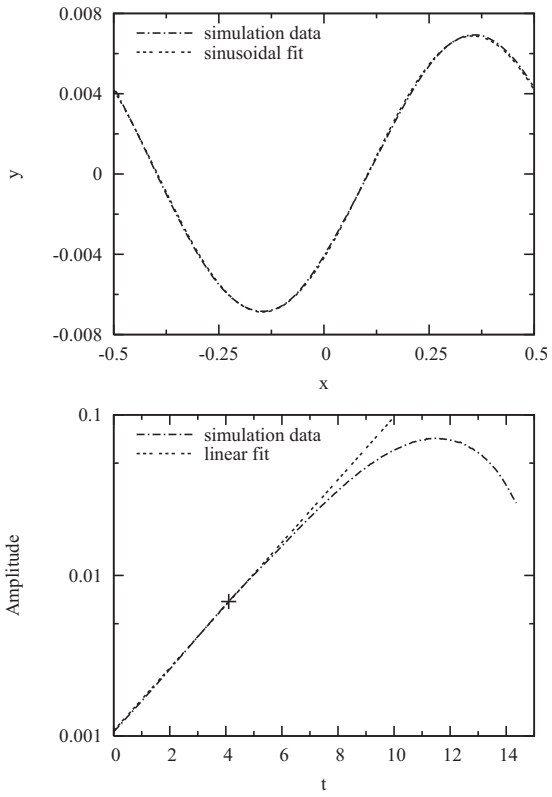

FIG. 3. Simulation and fitted profiles of the interface line (top) and time evolution of its amplitude (bottom). The interface line on the left is at time $t\approx4$ ("+" on the right plot).

In Fig. 4 we compare the numerical results obtained with GERRIS and the theoretical growth rates from the viscous and inviscid linear stability formulations, respectively, given by Eqs. (9) and (10) and Eqs. (13) and (14), for the four cases of Table I. The simulation results correctly predict the nondimensional growth rate (αc_i) of the linear stability theory. Notice that the viscous and inviscid theories predict the same behavior at small wavenumbers $\alpha\delta_g$. For case A, characterized by a surface tension coefficient equal to zero, the average percentage difference between the growth rates at different $\alpha\delta_g$ from the two different approaches is about 2%, while the maximum is about 9%. For case B, with the same physi-

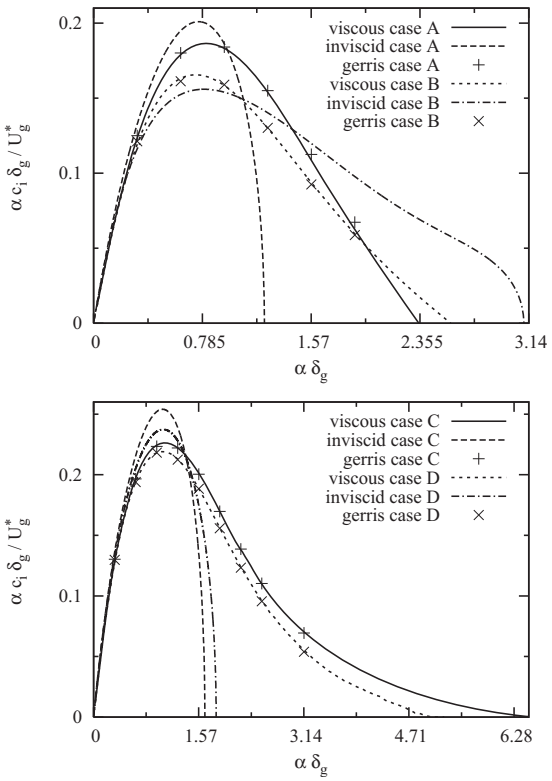

FIG. 4. Theoretical and numerical growth rates of the most unstable mode for cases *A* and *B* (top) and *C* and *D* (bottom) of Table I with a spatial resolution of 16 511 cells in the GERRIS code.

cal parameters as case *A* and with surface tension, the numerical and theoretical estimates of the growth rate are closer to each other and the mean difference goes down to about 0.8%. For cases *C* and *D*, the results are consistently better. The mean percentage difference between the growth rates computed from the initial-value problem and the viscous linear stability theory at different $\alpha\delta_g$ is about 0.45% without surface tension and 0.6% when surface tension is included. Thus we can conclude that at moderate density and viscosity ratios, the results obtained with GERRIS compare favorably with the growth rates from the linear stability eigenvalue problem.

Both codes, GERRIS and SURFER implement a direction-split VOF/PLIC algorithm, but they have some noticeable differences. In SURFER the advection and diffuse terms in the Navier–Stokes equation are discretized on a staggered grid with a simple centered finite-difference scheme in space, while the time-integration is fully explicit and first-order accurate. The surface tension term is implemented with the continuum-surface-stress approach[27] and the Poisson equation for the pressure is solved with a multigrid technique. In GERRIS variables are defined on a collocated grid. The advection term is estimated with a second-order unsplit upwind scheme,[29] with a Crank–Nicholson discretization of the viscous term. The CSF approach[30] for the capillary force has been implemented, with a curvature calculation based on the height function method. A staggered, second-order accurate time discretization is also considered.[14]

In Table III we report the percentage difference between the growth rates of the eigenvalue problem and the two initial-value codes for $\alpha\delta_g=\pi/2$ as a function of the grid resolution n_x, i.e., the number of cells along the x-coordinate. Although a reasonably good convergence with the mesh size is obtained with both codes, GERRIS always displays a better performance than SURFER. With GERRIS percentage differences less than 1% are obtained for the most refined meshes.

The error however ceases to decrease with mesh size in cases *B* and *D*, the two cases with surface tension. Thus the decrease of the error "saturates" around 1% for GERRIS. This "saturation" is not observed for SURFER, presumably because the 1% error level has not been reached with the grid resolutions of the table. We do not know the origin of this saturation. Because of extensive testing we exclude coding and algorithm errors. There are several remaining explanations for this kind of error: (a) the numerical method, although properly coded, could be intrinsically nonconvergent, (b) nonlinear effects could pollute the measurement of the growth rate obtained from the linearized equations, (c) other linear modes than the one initialized could pollute the measurements, and (d) the time evolution of the base flow creates errors.

We believe that (a) is likely: the method may be not convergent because the surface tension and the density and viscosity jumps create a singularity on the interface which is only partially accounted for by our method. For instance, the methods used for the estimation of the viscous effects do not take into account the fact that the velocity gradient has a jump. However, the same remark holds for capillary waves, and in that case a better agreement with theory is reported, of

TABLE III. Percentage difference of the growth rate for the four cases of Table I between the eigenvalue problem and the GERRIS and SURFER codes, for grid resolutions, $n_x=16$, 32, 64, 128, and 256, and wavenumber $\alpha\delta_g=\pi/2$. At the lowest resolutions we cannot always extract a meaningful growth rate from the simulation data.

	Code								
	GERRIS					SURFER			
Case	16	32	64	128	256	32	64	128	256
A	⋯	21.33	10.74	3.50	1.5	⋯	22.87	10.47	5.82
B	⋯	7.30	1.28	0.48	1.04	⋯	29.43	20.47	13.94
C	3.00	1.17	0.24	0.14	0.09	33.21	16.72	8.63	4.32
D	3.98	1.39	0.76	0.07	0.54	33.49	16.1	8.67	6.19

TABLE IV. Physical and geometrical parameters of the base flow profiles at large density and viscosity ratios.

Case	m	r	δ_l/L	δ_g/L	Re_l	Re_g	We_l	We_g
E	0.01	0.001	1/8	1/8	200	2000	∞	∞
F	0.01	0.001	1/8	1/8	20 000	2000	100 000	100

the order of 0.1% or better.[14] Nevertheless, it is possible that for a different testing procedure, the nonconvergence could appear at higher or lower accuracy. (b) Nonlinear effects should show as a progressive deviation from the straight line in amplitude plots. We have not seen such effects, although at the 1% level they could not be visible. One option would be to reduce the range of amplitudes in which the growth rate is measured, but this would also reduce the accuracy of the growth rate measurement. (c) Other slowly decaying linear modes are present and although we take care to initialize the system purely with the single unstable mode, some numerical effects trigger a low-amplitude excitation of the other modes. We somewhat reduced this effect but not completely. (d) The time evolution of the base flow is diminished when the Reynolds number is increased. We did not see a significant change in the results as the Reynolds number was varied.

IV. SIMULATIONS WITH LARGE DENSITY AND VISCOSITY RATIOS

In many practical applications, the density and viscosity ratios are large. In this section we present the results of the eigenvalue problem and the numerical simulations with GERRIS for a case where we decrease the viscosity ratio by one order of magnitude, $m=\mu_g/\mu_l=0.01$, and the density ratio by two orders of magnitude, $r=\rho_g/\rho_l=0.001$. The surface tension coefficient σ is either zero or 2.5×10^{-3} J/m^2. The value of the other relevant physical parameters, i.e., ρ_g, μ_g, δ_g, and U_g, is that of the previous section. The dimensionless numbers for these two tests are given in Table IV.

In Fig. 5 we compare the numerical results obtained with GERRIS and the theoretical growth rates from the viscous and inviscid linear stability formulations for the two cases of Table IV. Despite the large density and viscosity ratios, the numerical simulations still provide a good approximation of the growth rate (αc_i) of the most unstable mode. However, we remark the fact that it is more and more difficult to reproduce the theoretical results when both the wavenumber α and the surface tension coefficient σ are increased. Indeed, we reach a condition where the amplitude of the interface perturbation does not present a regime of linear growth rate, as in the case of Fig. 3, but where the amplitude continuously oscillates in time and we cannot compute the growth rate.

An interesting feature of the spectrum of the most unstable mode is the separation between the viscous and inviscid branches as the wavenumber increases, as shown in the zoomed area of Fig. 5. The curvature changes its sign twice, this being a rather stable feature that does not depend on the number N of Chebyshev polynomials.

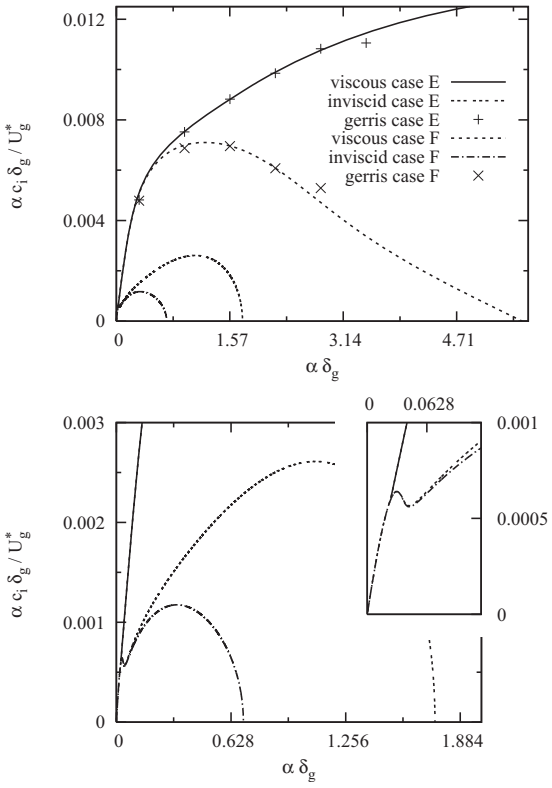

FIG. 5. Theoretical and numerical growth rates of the most unstable mode for cases E and F of Table IV (top) and local zoom where the viscous and inviscid curves separate from each other (bottom).

Another important issue of this set of simulations is the convergence of the growth rate with mesh refinement, as shown in Table V for $\alpha\delta_g=\pi/2$. We observe that the percentage difference of the growth rate is close to the value found at moderate density and viscosity ratios only at the highest resolution, i.e., $n_x=256$. In order to understand this behavior we show in Fig. 6 the profile for case E of the real ϕ_r and imaginary ϕ_i components of the eigenfunction $\phi(y)$. Notice that the eigenfunction changes very rapidly as it crosses the interface at $y=0$ from the liquid ($y<0$) to the gas ($y>0$) phase. Therefore, it is necessary to resolve adequately these spatial variations with approximately 256 grid cells in order to have a percentage difference of the order of 1% (see Fig. 6). As an alternative approach, one can also consider a more refined, adaptive grid near the interface. The accuracy and efficiency of this technique will be discussed in the next section.

TABLE V. Percentage difference of the growth rate for the two cases of Table IV between the eigenvalue problem and GERRIS, for maximal grid resolutions, $n_x=32$, 64, 128, and 256, and wavenumber $\alpha\delta_g=\pi/2$. At the lowest resolution we cannot extract a meaningful growth rate from the simulation data.

Case	32	64	128	256
E	⋯	59.11	27.05	0.13
F	⋯	54.95	14.11	0.05

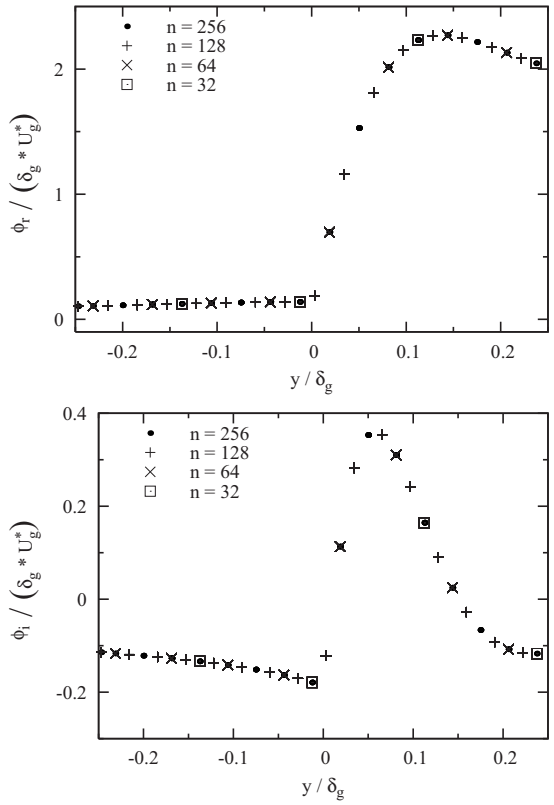

FIG. 6. Real (top) and imaginary (bottom) components of the eigenfunction $\phi(y)$ for case *E* of Table IV.

V. EFFICIENCY OF ADAPTIVE MESH REFINEMENT

In the previous section we have pointed out the need of grid refinement near the interface to resolve very steep changes of the eigenfunction. In the present section we investigate the performance of the tree-based AMR implemented in GERRIS. We consider again the four cases of Table I and a computational domain with three boxes in the vertical direction each of them with 256^2 square cells, for a total of $N_c = 196\,608$ cells with a uniform mesh. With AMR we consider a basic coarse resolution of 16^2 cells in each box and allow up to four additional levels of adaptive refinement, in order to have locally the same resolution of the fixed and uniform mesh. We maintain this high resolution in a wide band around the interface.

In Table VI, we provide the CPU time T for 100 time steps of a simulation. With AMR we exclude the first ten steps of the simulation. This is because the initial step and a few of the following step are at highest resolution in the entire domain, while after these few steps the grid settles to the desired adaptation. This biases the quantification of the number of cells N_c which is an important component of the measurements below. Indeed an interesting measure is the number of cells processed in one second, or per-cell speed, defined as

$$Z = \frac{nN_c}{T}, \tag{26}$$

where N_c is the average number of grid cells and n is the number of time steps. A simulation with AMR will have fewer cells and a smaller CPU time with respect to a uniform mesh with the highest resolution, but also a different per-cell speed. Therefore, it is interesting to compare the two per-cell velocities by defining their ratio η as the "efficiency" of adaptation, $\eta = Z_{\mathrm{AMR}}/Z$. One would expect that on a uniform grid without AMR the per-cell speed would be higher, but Table VI shows that the opposite is true: efficiency is larger than one, so that adaptative simulations are faster by nearly a factor 3/2 on the small meshes. The reason for this unexpected behavior is currently under investigation.

The results of Table VI show that the per-cell speed of SURFER is approximately 20 times larger than that of GERRIS, for a given test case and same mesh. However it may be more interesting to compare the results at similar accuracy rather than at the same number of cells. Then in many cases GERRIS turns out to be more efficient.

VI. CONCLUSIONS

Numerical simulations of the instability evolution of a viscous shear layer have been performed with GERRIS, an adaptive mesh refinement code based on the volume of fluid method. Good agreement between the growth rates predicted by the linear eigenvalue problem and the nonlinear initial-value problem solved by GERRIS is found for moderate density and viscosity ratios with a good convergence with grid refinement.

For large density and viscosity ratios, it is more and more difficult to compute the growth rate of the instabilities as the wavenumber and the surface tension coefficient increase. The main reason for this behavior is the fact that the complex eigenfunctions develop very steep gradients near the equilibrium interface and many grid points are there necessary to resolve adequately the eigenfunctions. If high ac-

TABLE VI. Average number of cells N_c and CPU times T for the two codes GERRIS and SURFER, for case *A* of Table I, with different grid resolutions n_x and wavenumber $\alpha\delta_g = \pi/2$.

	Code						
	GERRIS					SURFER	
n_x	$(N_c)_{\mathrm{AMR}}$	T_{AMR}	N_c	T	η	N_c	T
32	1727	3.19	3072	8.97	1.58	3072	0.47
64	4607	11.37	12 288	46.29	1.53	12 288	1.83
128	16 511	50.71	49 152	190.54	1.26	49 152	8.46
256	62 847	212.75	196 608	834.25	1.25	196 608	32.4

curacy is necessary then AMR is required in these conditions in order to keep the grid size and the computational time reasonable.

[1] J. C. Lasheras and E. J. Hopfinger, "Liquid jet instability and atomization in a coaxial gas stream," Annu. Rev. Fluid Mech. **32**, 275 (2000).

[2] P. G. Drazin, *Introduction to Hydrodynamic Stability* (Cambridge University Press, Cambridge, 2002).

[3] C. S. Yih, "Instability due to viscosity stratification," J. Fluid Mech. **27**, 337 (1967).

[4] A. P. Hooper and W. G. C. Boyd, "Shear–flow instability at the interface between two viscous fluids," J. Fluid Mech. **128**, 507 (1983).

[5] E. J. Hinch, "A note on the mechanism of the instability at the interface between two shearing fluids," J. Fluid Mech. **144**, 463 (1984).

[6] F. X. Keller, J. Li, A. Vallet, D. Vandromme, and S. Zaleski, "Direct numerical simulation of interface breakup and atomization," in *Proceedings of ICLASS'94*, edited by A. J. Yule (Beggell, New York, 1994), pp. 56–62.

[7] J. Li, "Calcul d'interface affine par Morceaux (piecewise linear interface calculation)," C. R. Acad. Sci., Ser. IIb: Mec., Phys., Chim., Astron. **320**, 391 (1995).

[8] A. Leboissetier and S. Zaleski, "Influence des conditions amont turbulentes sur l'atomisation primaire," Combustion **2**, 75 (2002) (Revue des Sciences et Techniques de Combustion).

[9] W. Tauber, S. O. Unverdi, and G. Tryggvason, "The non–linear behavior of a sheared immiscible fluid interface," Phys. Fluids **14**, 2871 (2002).

[10] P. Yecko, S. Zaleski, and J.-M. Fullana, "Viscous modes in two–phase mixing layers," Phys. Fluids **14**, 4115 (2002).

[11] T. Boeck and S. Zaleski, "Viscous versus inviscid instability of two–phase mixing layers with continuous velocity profile," Phys. Fluids **17**, 032106 (2005).

[12] S. Popinet, "Gerris: A tree–based adaptive solver for the incompressible Euler equations in complex geometries," J. Comput. Phys. **190**, 572 (2003).

[13] M. M. Francois, S. H. Cummins, E. D. Dendy, D. B. Kothe, J. M. Sicilian, and M. W. Williams, "A balanced–force algorithm for continuous and sharp interfacial surface tension models within a volume tracking framework," J. Comput. Phys. **213**, 141 (2006).

[14] S. Popinet, "An accurate adaptive solver for surface-tension-driven interfacial flows," J. Comput. Phys. **228**, 5838 (2009).

[15] D. Fuster, A. Bagué, T. Boeck, L. Le Moyne, A. Leboissetier, S. Popinet, P. Ray, R. Scardovelli, and S. Zaleski, "Simulation of primary atomization with an octree adaptive mesh refinement and VOF method," Int. J. Multiphase Flow **35**, 550 (2009).

[16] T. Boeck, J. Li, E. López-Pagés, P. Yecko, and S. Zaleski, "Ligament formation in sheared liquid–gas layers," Theor. Comput. Fluid Dyn. **21**, 59 (2007).

[17] A. Michalke, "On spatially growing disturbances in an inviscid shear layer," J. Fluid Mech. **23**, 521 (1965).

[18] M. Gaster, "A note on the relation between temporally–increasing and spatially–increasing disturbances in hydrodynamic stability," J. Fluid Mech. **14**, 222 (1962).

[19] R. C. Lock, "The velocity distribution in the laminar boundary layer between parallel streams," Q. J. Mech. Appl. Math. **4**, 42 (1951).

[20] P. A. Monkewitz and P. Huerre, "Influence of the velocity ratio on the spatial instability of mixing layers," Phys. Fluids **25**, 1137 (1982).

[21] T. Boeck and S. Zaleski, "Instability of two–phase mixing layers: Analysis of exact and approximate base flows from boundary layer theory," J. Non-Equilib. Thermodyn. **30**, 215 (2005).

[22] J. P. Boyd, "Orthogonal rational functions on a semi–infinite interval," J. Comput. Phys. **70**, 63 (1987).

[23] P. A. M. Boomkamp, B. J. Boersma, R. H. M. Miesen, and G. V. Beijnon, "A Chebyshev collocation method for solving two–phase flow stability problems," J. Comput. Phys. **132**, 191 (1997).

[24] P. J. Schmid and D. S. Henningson, *Stability and Transition in Shear Flows* (Springer, New York, 2001).

[25] S. A. Orszag, "Accurate solution of the Orr–Sommerfield stability equation," J. Fluid Mech. **50**, 689 (1971).

[26] C. B. Moler and G. W. Stewart, "Algorithm for generalized matrix eigenvalue problems," SIAM (Soc. Ind. Appl. Math.) J. Numer. Anal. **10**, 241 (1973).

[27] B. Lafaurie, C. Nardone, R. Scardovelli, S. Zaleski, and G. Zanetti, "Modelling merging and fragmentation in multiphase flows with SURFER," J. Comput. Phys. **113**, 134 (1994).

[28] D. Gueyffier, A. Nadim, J. Li, R. Scardovelli, and S. Zaleski, "Volume of fluid interface tracking with smoothed surface stress methods for three–dimensional flows," J. Comput. Phys. **152**, 423 (1999).

[29] J. Bell, P. Colella, and H. Glaz, "A second-order projection method for the incompressible Navier–Stokes equations," J. Comput. Phys. **85**, 257 (1989).

[30] J. Brackbill, D. Kothe, and C. Zemach, "A continuum method for modeling surface tension," J. Comput. Phys. **100**, 335 (1992).

AUTHOR QUERIES — 035008PHF

#1 Au: Please provide zip codes for the second and third affiliations.
#2 Au: Please check changes in the title and affiliations.
#3 Au: Please provide the correct definition of ″PLIC″ if possible.
#4 Au: Please provide the correct definition of ″NAG″ if possible.
#5 Au: Please check changes in sentence “However, the same remark…” if your meaning was preserved.
#6 Au: Please provide the correct definition of ″CPU″ if possible.
#7 Au: Please verify volume in Ref. 3.
#8 Au: Please provide full journal title, ISSN, and/or CODEN of Reference 8.
#9 Au: Please verify year in Ref. 20.
#10 Au: Please check number in boldface in Table II.